A R C H I V E S O F M E T A L L U R G Y A N D M A T E R I A L S
Volume 57 2012 Issue 2
DOI: 10.2478/v10172-012-0047-y

K. LI*, M. SONG*, Y. DU*, X. FANG*

EFFECT OF MINOR CU ADDITION ON THE PRECIPITATION SEQUENCE OF AN AS-CAST Al-Mg-Si 6005 ALLOY

WPŁYW NIEWIELKIEJ ZAWARTOŚCI MIEDZI NA SEKWENCJĘ WYDZIELEŃ W ODLEWANYCH STOPACH Al-Mg-Si 6005

The whole precipitation sequences of two as-cast Al-Mg-Si 6005 alloys (containing no Cu or 0.1 wt.% Cu) at 150°C were investigated using X-ray diffraction, transmission electron microscopy and hardness examinations. The precipitation sequence of the Cu-free alloy can be expressed as: super-saturated solid solution (SSSS) → spherical G.P. zones → pre-β'' → β'' → U2 + Si +β_x → Si +β_x, while that of the Cu-containing alloy can be expressed as: SSSS → spherical G.P. zones + platelet-like G.P. zones → pre-β'' → β'' → Q′ + β+ Si → Q +β+ Si. A new type of β precipitate, namely β_x here, has been discovered in the Cu-free alloy. The addition of minor Cu is found to accelerate the microstructural evolution by inducing the formation of a new type of platelet-like G.P. zone along $\{111\}_{Al}$ planes, and improve the hardening response at the over-aged stage by forming Q′ and Q precipitates.

Keywords: aluminum alloys, precipitation, ageing, phase transformation

Kompletna sekwencja wydzieleń dwóch odlanych stopów Al-Mg-Si 6005 (zawierających 0 i 0.1%.wag Cu), w temperaturze 150°C, została zbadana przy użyciu dyfrakcji rentgenowskiej, transmisyjnej mikroskopii elektronowej i badań twardości. Sekwencja wydzieleń w stopie nie zawierającym Cu może być przedstawiona następująco: przesycony roztwór stały → sferyczne strefy Guiniera-Prestona → pre-β'' → β'' → U2 + Si + β_x → Si +β_x, natomiast dla stopu zawierającego Cu następująco: przesycony roztwór stały → sferyczne i płytkowe strefy Guiniera-Prestona → pre-β'' → β'' → Q′ + β+ Si → Q +β+ Si. Nowy rodzaj wydzieleń β, tj. β_x, został odkryty w stopie niezawierającym Cu. Stwierdzono, że dodatek niewielkiej ilości Cu przyspiesza zmiany mikrostruktury poprzez indukowanie tworzenia nowego typu płytkowych stref Guiniera-Prestona wzdłuż płaszczyzny $\{111\}_{Al}$ i poprawia utwardzenie poprzez tworzenie wydzieleń Q′ i Q.

1. Introduction

Al-Mg-Si alloys are widely used in motor and aircraft industries due to their excellent plasticity and corrosion resistance, light weight and medium strength after appropriate working processes (such as rolling and extrusion) and heat treatments including mainly solution, quenching and aging treatments. In recent years, the strengthening mechanisms of Al-Mg-Si alloys after various working processes and heat treatments have been studied by many researchers. During the aging treatment after working and solution treatment, solute atoms form atomic clusters or G.P. zones, after which needle/lath-like precipitates nucleate and finally stable precipitates form. The main precipitates formed in Al-Mg-Si alloys during aging treatment are listed in Tables 1 and 2 [1-21]. It is generally believed that the precipitation sequence of Al-Mg-Si alloys during aging can be expressed as [22]: super-saturated solid solution (SSSS) → atomic clusters → G.P. zones → pre-β'' → β'' → β'/U1/U2/B′ → β (stable). In general, the precipitation sequence of an Al-Mg-Si alloy depends on many parameters, among which the alloy composition is one of the most important factors. According to the study of Marioara et al. [22], the Mg/Si ratio of the dominant phase in an Al-Mg-Si alloy is close to that of the alloy, while the heat treatment parameters (solution temperature and time, aging temperature and time) will not modify the sequence of the dominant precipitates.

The effect of copper addition is also important since it will introduce the copper containing Q phase as well as its precursor Q′ into the sequence [23]. The Cu element was reported to segregate at the Q′/α-Al interface [24]. Due to the low diffusivity of Cu in α-Al, such a segregation would delay the coarsening of Q′, and thus the Al-Mg-Si-Cu alloys were reported with high thermal stability [25]. Moreover, alloys with higher Cu content were always reported more strengthened [23, 26]. With the

* STATE KEY LABORATORY OF POWDER METALLURGY, CENTRAL SOUTH UNIVERSITY, CHANGSHA 410083, CHINA

TABLE 1

Summary of the ante-β'' and β'' precipitates reported in Al-Mg-Si(-Cu) alloys

Precipitate type	Atomic ratio	Morphology characteristics	Space group and crystal parameters (nm)	Orientation relationships	Other characteristics
spherical G.P. zones (Atomic Clusters)	Mg and Si clusters and co-clusters, Mg:Si ratio of ~1:1 [1]. The Mg:Si ratio is close to that of the alloy composition [2].	Fine particles with a Size of ~2 nm [2].	No distinct structure [3].	/	Fully coherent with Al matrix, designated as spherical G.P. zones, not observable by HRTEM [1, 2, 3].
Plate-like G.P. zones	Si/Mg = 1.	Platelet along $\{001\}_{Al}$ planes	(fcc L10), a = 0.405 [4].	Elongating along $<100>_{Al}$ directions.	Fine plates of a monolayer in thickness, with a width of about 2.5 nm and a length of less than 30 nm.
Pre-β''	$(Al+Mg)_5Si_6$.	Needles along $<001>_{Al}$.	The structure resembles that of β'' with different positions for some of the Mg atoms along the needle direction.	/	The structure is more similar to the Al matrix than β''. With the Al replaced by Mg and Si, this phase developes as β'' [5].
β'' (G.P.-II zone)	Mg_5Si_6 [6] or Mg/Si = 1.1 with ~20 at. % Al [7].	Needles along $<001>_{Al}$.	C2/m, a = 1.516, b = 0.405, c = 0.674, β = 105.3° [6].	$[100]_{\beta''}$// $[230]_{A1}$, $[010]_{\beta''}$// $[001]_{Al,}$ $[001]_{\beta''}$// $[\bar{3}10]_{Al}$ [6].	Streaks around the needles caused by its stress field in the Al matrix around it [6~8].
	Al_3MgSi_6 [8].	Needles along $<001>_{Al}$.	P2/m, a = 0.77±0.02, b = 0.67±0.01, c = 0.203, γ = 75 ± 0.5° [8].	$(001)_{\beta''}$// $(001)_{Al}$, $[100]_{\beta''}$// $[310]_{Al}$ [8].	

improved thermal stability and elevated strength, the Al-Mg-Si-Cu alloys are of widespread industrial interest. However, previous studies mainly investigated alloys with Cu additions higher than 0.2 wt. %, few work were focused on the effect of minor Cu addition on the whole precipitation sequence, i.e. from SSSS to the stable phases.

In this work, we focus on the effect of minor Cu on the microstructural evolution of an as-cast Al-Mg-Si alloy (composition close to 6005 aluminum alloy). To simplify the problem, no working process was applied to the alloys to avoid excessive dislocations in the Al matrix, which might be the sites for the nucleation of B′ [22] and Q [27] precipitates. The solution treatment at 550°C for 4 hours was used to increase the grain size (determined as 100~500 μm by optical microscopy obsevation) and eliminate the influence of the grain boundary because the Q precipitates in Al-Mg-Si-Cu alloys were reported to nucleate along the dislocations and grain boundaries [27].

TABLE 2

Summary of the post-β'' precipitates reported in Al-Mg-Si(-Cu) alloys

Precipitate type	Atomic ratio	Morphology characteristics	Space group and crystal parameters (nm)	Orientation relationships	Other characteristics
β'	Mg_9Si_5.	Rods along $<001>_{Al}$.	$P6_3/m$, a = b = 0.715, c = 1.215, γ = 120°[9].	$[001]_{\beta'}$// $[001]_{Al}$, $[1\bar{1}0]_{\beta'}$// $[\bar{3}10]_{Al}$ [9].	
U1 (type-A)	$MgAl_4Si_5$ (type-A) [8,10].	Needles along $<001>_{Al}$.	$P\bar{6}2m$, a = b = 0.405, c = 0.67, [8,10].	$(\bar{1}2\bar{1}0)_A$// $(001)_{Al}$, $[0001]_A\hat{}[100]_{Al}$ = 20° [8,10].	Octagonal shape and largest diameter and length of all the metastable phases [8,10].
	$MgAl_2Si_2$ (U1) [11].		$P\bar{3}m1$, a= b= 0.405, c= 0.674, γ = 120° [11].	$[001]_{Al}$//$[100]_{U1}$, $[310]_{Al}$//$[001]_{U1}$, $[1\bar{3}0]_{Al}$//$[120]_{U1}$ [11].	
U2 (type-B)	$Mg_2Al_4Si_5$ (type-B) [8,10].	Rods along $<001>_{Al}$.	Pnma, a = 0.675, b = 0.405, c = 0.794 [8,10~12].	$(001)_B$// $(001)_{Al}$, $[010]_B\hat{}[010]_{Al}$ = 20° [8].	Note that the difference between the two orientation relationships is within the limit of experimental error.
	MgAlSi (U2) [11,12].			$(001)_{Al}$// $(010)_{U2}$, $[\bar{3}10]_{Al}$// $[100]_{U2}$, $[130]_{Al}$// $[001]_{U2}$ [12].	

cd TABLE 2

B′ (type-C)	Mg/Si~1 [8,10,13].	Laths along $<001>_{Al}$.	Hexagonal, a = 1.04, c = 0.405, $\gamma = 120°$ [10,13].	$(0001)_C$// $(001)_{Al}$, $[2\bar{1}\bar{1}0]_C$ ^ $[100]_{Al}$ = 10° [8,10].	B′ shows similar hexagonal crystal lattice with Q′ [14].
Q′	$Al_4CuMg_6Si_6$.	Laths along $<001>_{Al}$.	Hexagonal, a = 1.04, c = 0.405 [14].	$[0001]_{Q'}$// $[001]_{Al}$, $[1\bar{2}10]_{Q'}$// $[130]_{Al}$.	$\{510\}_{Al}$ habit planes for the laths, metastable precursor of Q. More coherent with the matrix than Q.
Q	$Al_4Cu_2Mg_8Si_7$ [15].	Laths along $<001>_{Al}$.	$P\bar{6}$, a = b = 1.039, c = 0.402 [15].	$[0001]_Q$ // $[001]_{Al}$, $[\bar{1}\bar{1}20]_Q$ // $[510]_{Al}$ [16].	Stable phase, with $\{510\}_{Al}$ habit planes for the laths [16].
	$Al_5Cu_2Mg_8Si_6$ [16].		Hexagonal, a = 1.03, c = 0.4505 [16].		
β	Mg_2Si.	Platelet/cube shape.	$Fm\bar{3}m$, a = 0.635 [17], a = 0.633 [18].	Orientation 1 [18]: $\{001\}_\beta$// $\{001\}_{Al}$, $<100>_\beta$// $<110>_{Al}$. Orientation 2 [19]: $\{111\}_\beta$// $\{111\}_{Al}$, $<110>_\beta$// $<110>_{Al}$.	Observed in Cu-free alloys, octagon-like. Observed in Cu-containing alloys.
Si	Si.	Platelet-like, irregular shape	$Fd\bar{3}m$, a = 0.5431 [20].	Multiple orientation in α-Al matrix [21].	

2. Experimental

Two as cast Al-Mg-Si alloys with and without minor Cu addition (composition close to 6005 aluminum alloy) were used in the present study, and the compositions are given in Table 3. For each alloy, Ø17 mm×80 mm rods were casted from high-purity Al (99.9%), high-purity Mg (99.9%), Al-20.2 wt.% Si and Al-49.5 wt.% Cu master alloys using arc melting furnace under an argon atmosphere. In order to focus on the effect of minor Cu on the microstrutural evolution, no deformation process was performed on the alloys. Specimens with a size of Ø17 mm×8 mm were homogenized at 550°C for 4 h and subsequently quenched in ice water. The specimens were then stored at room temperature (RT) for less than 10 min before aging treatment at 150°C for different time (up to 10 days).

Brinell hardness examinations were performed on both alloys to study the mechanical responses of the alloys with aging time. Microstructural evolution and precipitation sequences of the alloys were studied using transmission electron microscope (TEM) and high resolution transmission electron microscope (HRTEM). The TEM specimens were cut (from the inner part of the Ø17 mm×8 mm specimens using electric discharge machine), grounded and mechanically polished with low speeds in a cooling fluid to avoid extra severe deformation and heating. The mechanically polished specimens were subsequently thinned by twin jet electro-polishing in a 30% nitric acid and 70% methanol solution at -30°C, and examined in a Tecnai G^2 20 TEM and a JEOL-3010 HRTEM operated at 200 kV. XRD examinations were performed on the specimens at the over-aged stage to analyze the irregular-shaped precipitates observed in the corresponding TEM images.

TABLE 3

Nominal/measured chemical compositions (wt. %) and nominal atomic ratios of the alloys

Alloy	Mg	Total Si	Cu	Fe	Zn	Al	Mg: Si: Cu (at. %)
1	0.55/0.57	0.7/0.69	0/0.007	0/0.02	0/0.008	Balance	0.91: 1: 0
2	0.55/0.59	0.7/0.73	0.10/0.087	0/0.014	0/0.005	Balance	0.91: 1: 0.063

3. Results

3.1. Hardness curves

Fig. 1 shows the effect of aging time on the Brinell hardness of the two alloys. The two hardness curves show great fluctuations at the under-aged stage, especially in the very beginning (aging time <5 h). The Cu-containing alloy has higher hardness values at the over-aged stage (aging time >60 h). The maximum hardening effect is supposed to occur between aging time 30h and 60h in both alloys based on the curvature of the hardness test result. There are two sharp decreases in hardness values for both alloys from 60 h to 90 h and from 120 h to 150 h, respectively.

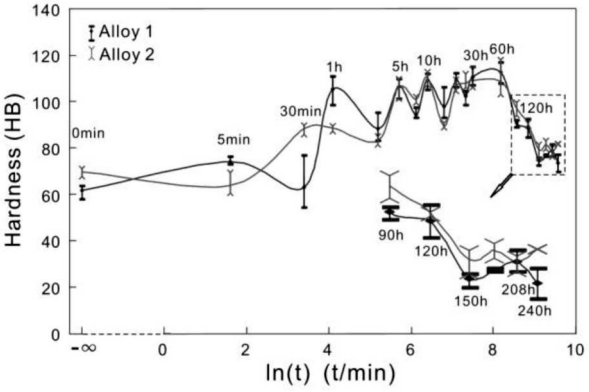

Fig. 1. Brinell hardness evolution of the alloys as a function of aging time

3.2. XRD patterns

The XRD patterns of alloys 1 and 2 aged for 120 h and 240 h are shown in Fig. 2. The patterns show low but distinct Si peaks with similar intensities for both alloys. It should be noted that the needle/rod/lath-like precipitates can hardly be detected by XRD due to the small volume fraction and small size of these precipitates embedded in the Al matrix.

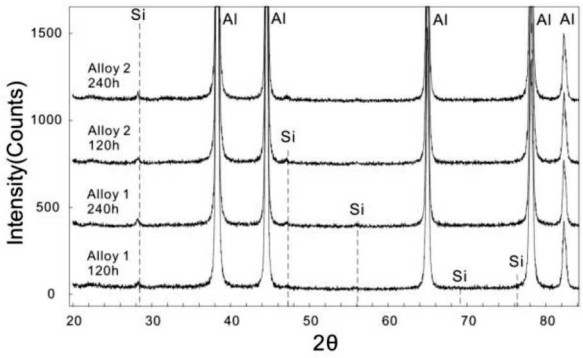

Fig. 2. Powder XRD curves of alloys 1 and 2 aged for 120 h and 240 h, respectively

3.3. TEM observations

Figs. 3a, 3c and 3e show the strain contrast caused by atomic clusters or spherical G.P. zones in alloy 1. In contrast, in Figs. 3b, 3d and 3f, apparent microstructural change from G.P. zones to β'' can be observed. One should be noted that the existence of β'' precipitates in Fig. 3f can further be confirmed by selected area diffraction pattern (SADP) calculations (method for SADP calculation can be found from [28]) based on its experimentally determined structural parameters and orientation relationship with α-Al matrix [6], as shown in Fig. 4a. The spherical G.P. zones observed in Figs. 3a, 3b and 3e are also visible in HRTEM, as shown in Figs. 3c~3d, showing a diameter of about 3~4 nm.

Figs. 3b and 5 show TEM image and HRTEM image of alloy 2 aged for 5 min, taken along the zone axis of $[110]_{Al}$. Two kinds of contrast shapes are observed with needle-like and platelet morphologies. Based on the concept of 3D topology and the same length (6 nm) of these two shapes, it is concluded that these shapes belong to the same kind of precipitate: platelet-like G.P. zones parallel to $\{111\}_{Al}$. The needle-like shapes, marked by black arrows in Fig. 5, are the side views of the platelets along $(1\bar{1}1)_{Al}$, which is parallel to the zone axis. The platelet-like shapes, marked by dashed frames in Fig. 5, are the projections of the platelets parallel to $(111)_{Al}$ or $(11\bar{1})_{Al}$, which have a projection angle of 35° with the $(110)_{Al}$ plane (i.e. the normal plane). The size distribution of the G.P. platelets is from 6 nm to 12 nm (see Fig. 3b), with 1~5 layers of atoms in thickness (see Fig. 5).

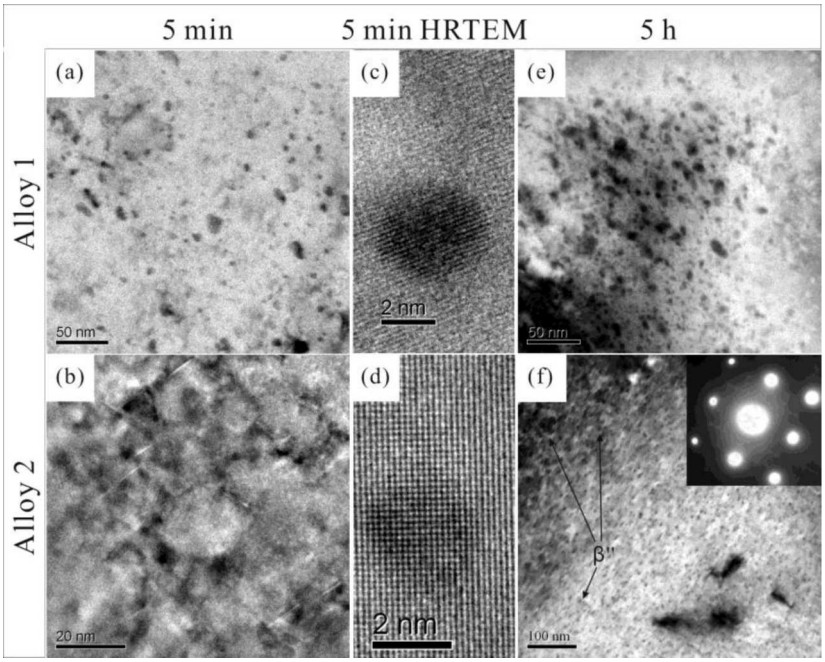

Fig. 3. TEM bright field images of the under-aged specimens: (a) alloy 1 aged for 5 min, Z = $[110]_{Al}$, (b) alloy 2 aged for 5 min, Z = $[110]_{Al}$, (c) HRTEM image of alloy 1 aged for 5 min, Z = $[110]_{Al}$ and (d) HRTEM image of alloy 2 aged for 5 min, Z = $[001]_{Al}$, (e) alloy 1 aged for 5 h, Z = $[001]_{Al}$, (f) alloy 2 aged for 5h, Z = $[001]_{Al}$

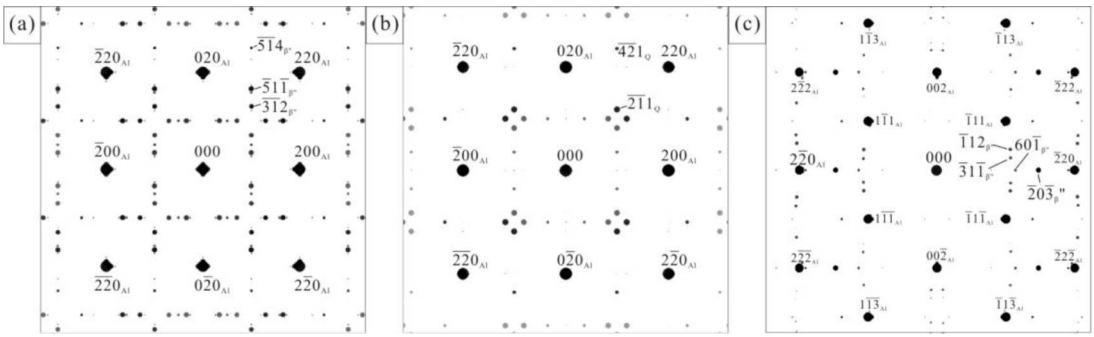

Fig. 4. Calculated composite SADPs for (a) β'' precipitates in α-Al matrix, Z = $[001]_{Al}$, (b) Q′/Q precipitates in α-Al matrix, Z = $[001]_{Al}$, and (c) β'' precipitates in α-Al matrix, Z = $[110]_{Al}$

Fig. 3f shows a bright field image of alloy 2 aged for 5 h taken along the zone axis of $[001]_{Al}$, which is the most representative direction for the observation of precipitates in Al-Mg-Si alloys. High density of short primary needle-like β'' precipitates (average length of 9 nm and width of 4 nm) can be seen along $<100>_{Al}$ directions. Similar features are observed in alloy 1 aged for 10 h and 30 h, as presented in Fig. 6. Fig. 6a shows dim and short needle-like precipitates. The corresponding SADP (inset in Fig. 6a) only shows separated dim spots among the bright Al spots as well as spots from double diffraction, different with those in Fig. 3f and Fig. 4a. According to the work of Chen et al. [29], the transformation from G.P. zones to β'' precipitates is accompanied with the evolution of both structure and composition. Therefore these precipitates can be regarded as intermediate products between the G.P. zones and β'' precipitates, i.e. pre-β''. Fig. 6b shows the well developed needle-like β'' precipitates with an average length of 14 nm. The SADPs inset in Figs. 3f and 6b were also observed previously [23, 30], and are successfully calculated in Fig. 4a.

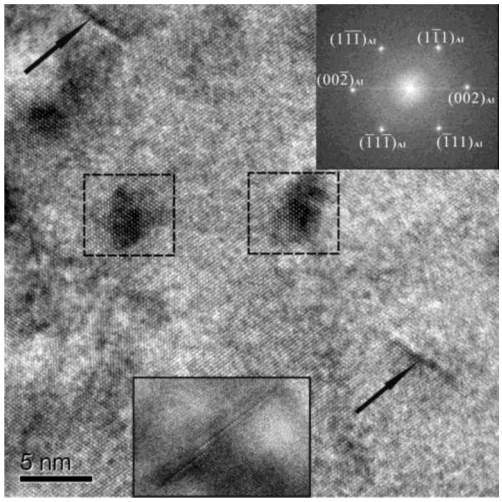

Fig. 5. A HRTEM image of alloy 2 aged for 5 min, Z = $[110]_{Al}$. The FFT image is indexed and given as an upper right corner inset. The two black arrows mark the side views of two G.P. platelets parallel to $(1\bar{1}1)_{Al}$, while in the two dashed frames are the projections of the G.P. platelets parallel to $(111)_{Al}$ or $(11\bar{1})_{Al}$. The black solid frame marks a G.P. platelet parallel to $(\bar{1}11)_{Al}$ in another field of the same grain

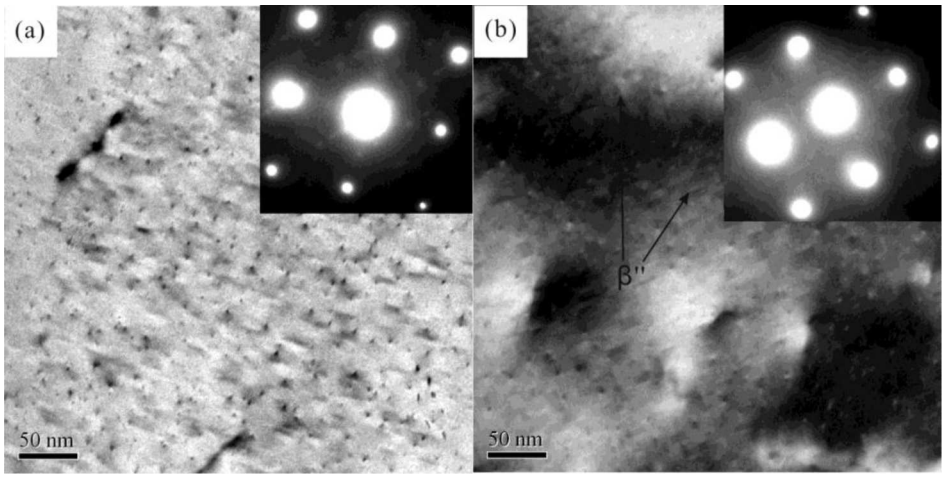

Fig. 6. TEM bright field images and corresponding SADPs (the insets) of alloy 1 aged for (a) 10h and (b) 30h, Z = $[001]_{Al}$

Long needle-like precipitates, short rod-like precipitates, platelet-like precipitates and fine irregular-shaped particles are observed in alloy 1 aged for 120 h, as shown in Fig. 7. The needle-like precipitates, with a length distribution from 50 nm to 300 nm and a uniform width of 5 nm, are the mature β'' precipitates. The rod-like precipitates have a width distribution from 7 nm to 10 nm, and a length distribution from 50 nm to 170 nm. According to the morphology of U2 precipitates observed by Marioara et al. [22], these rod-like precipitates are U2 precipitates. The fine particles, with a size distribution from 10 to 30 nm, are confirmed as the initial Si crystals by the Si peaks in the XRD pattern for alloy 1 aged for 120h in Fig. 2. The platelet-like precipitates are near parallel to $(002)_{Al}$ with a tilting angle of about 2.3° (marked by arrows in Fig. 7), and have an un-equilateral octagonal shape (see the inset in the upright corner of Fig. 7). As its opposite borders are parallel to each other, it can be concluded that the platelet-like precipitate have four couples of growth directions. None of the borders is parallel to $<100>_{Al}$ or $<110>_{Al}$, and an angle of 8° is denoted in the inset of Fig. 7. According to the similarity in morphology and the difference in orientation between β_x platelet in this work and the β platelet observed by Matsuda et al. [18], β_x is another type of the β platelet-like precipitate, which was reported parallel to $\{001\}_{Al}$ and growing along $<100>_{Al}$ directions. However, further study is needed before exactly identifying the structure and orientation characteristics of β_x.

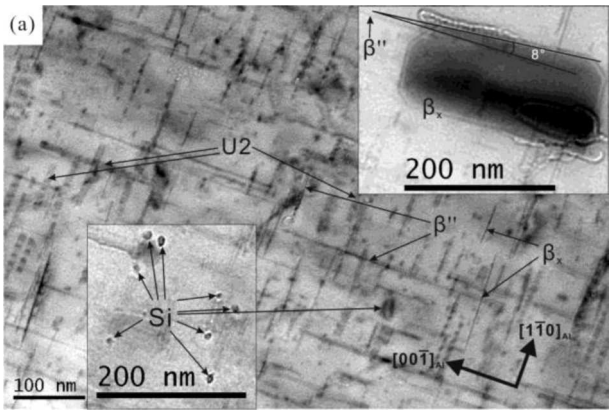

Fig. 7. TEM bright field images of alloy 1 aged for 120 h, Z = $[110]_{Al}$. Inset in the lower left corner is the image of Si particles, and inset in the upper right corner is the image of an β_x platelet. All the images were taken in the same grain

In alloy 1 aged for 208 h and 240 h, both hexagonal and irregular shapes of the Si crystals are observed, as shown in the bright field images in Fig. 8, and further confirmed by the corresponding SADP (see the insets in Fig. 8) and XRD patterns (see Fig. 2). Streaks caused by needle-like β'' precipitates can also be seen in the SADPs inset in Fig. 8 (see the spots in the white dashed frame), and are reproduced by SADP calculation, as shown in Fig. 4c. The residual rod-like U2 precipitates and needle-like β'' precipitates in alloy 1 aged for 208 h and 240 h are shorter than those in alloy 1 aged for 120 h, revealing their dissolution after aging time of 120h.

Compared to alloy 1, the precipitates in alloy 2 aged for 120 h and 240 h shows different morphologies (see Fig. 9). β, Q′, β'' and Si crystals are observed in alloy 2 aged for 120 h. The lath-like Q′ precipitates show similar morphology with those observed by Miao and Laughlin [23], and Yassar et al. [30], with similar spots in the corresponding SADP patterns. The elongation direction of the Q′ precipitate is parallel to $<100>_{Al}$, while the width direction is off $<100>_{Al}$ by an angle of about 11 degrees, indicating a habit plane of $\{510\}_{Al}$, a characteristic habit plane of Q′ and Q precipitates described by previous studies [14,16]. The Q′ precipitate is confirmed by calculating the corresponding SADP (see Fig. 4b) based on the structural information reported previously [15], as listed in Table 2.

In alloy 2 aged for 240 h (see Fig. 9c), the long lath-like precipitates have more faint morphologies than those in alloy 2 aged for 120 h, revealing the stronger stress field caused by the mismatch between c_Q =0.402 nm [15] and a_{Al} =0.405nm. The habit plane of $\{510\}_{Al}$ is identified for the Q precipitates. The diffraction spots due to the Q precipitates in the SADP of alloy 2 aged for 240 h (see Fig. 9d) are confirmed by SADP calculation (see Fig. 4b). The Si crystals present both hexagonal and irregular morphologies, and rings of $\{111\}_{Si}$, $\{220\}_{Si}$, $\{113\}_{Si}$ are shown in Figs. 8 and 9, revealing that the Si crystals have many orientations or random orientation in the α-Al matrix. The fraction of Si crystals in alloy 2 aged for 240 h is much larger than that in alloy 2 aged for 120 h, and the β'' precipitate is no longer observed in alloy 2 aged for 240 h.

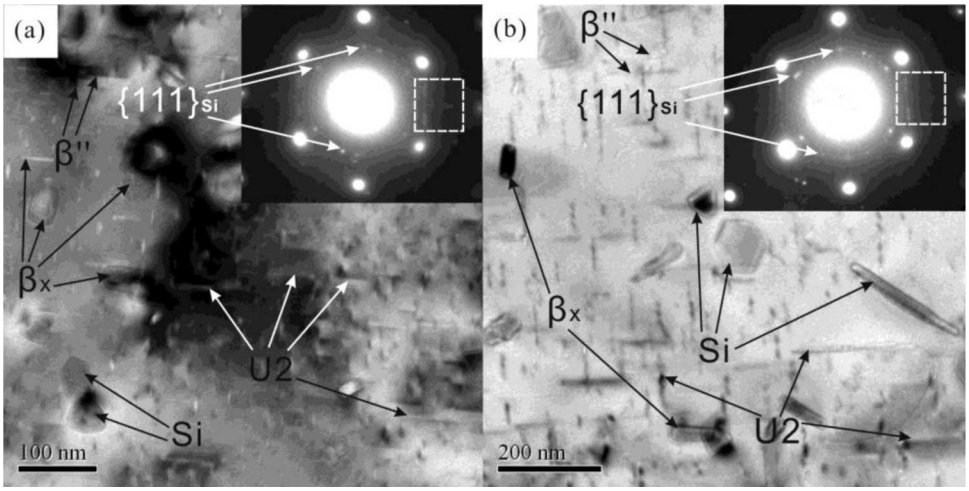

Fig. 8. TEM bright field images of (a) alloy 1 aged for 208 h and (b) alloy 1 aged for 240 h with Z = $[110]_{Al}$. It should be noted that the polycrystalline rings due to Si crystals are clearly observed in the inset SADPs. In the white dashed frames are the streaks caused by needle-like β'' precipitates

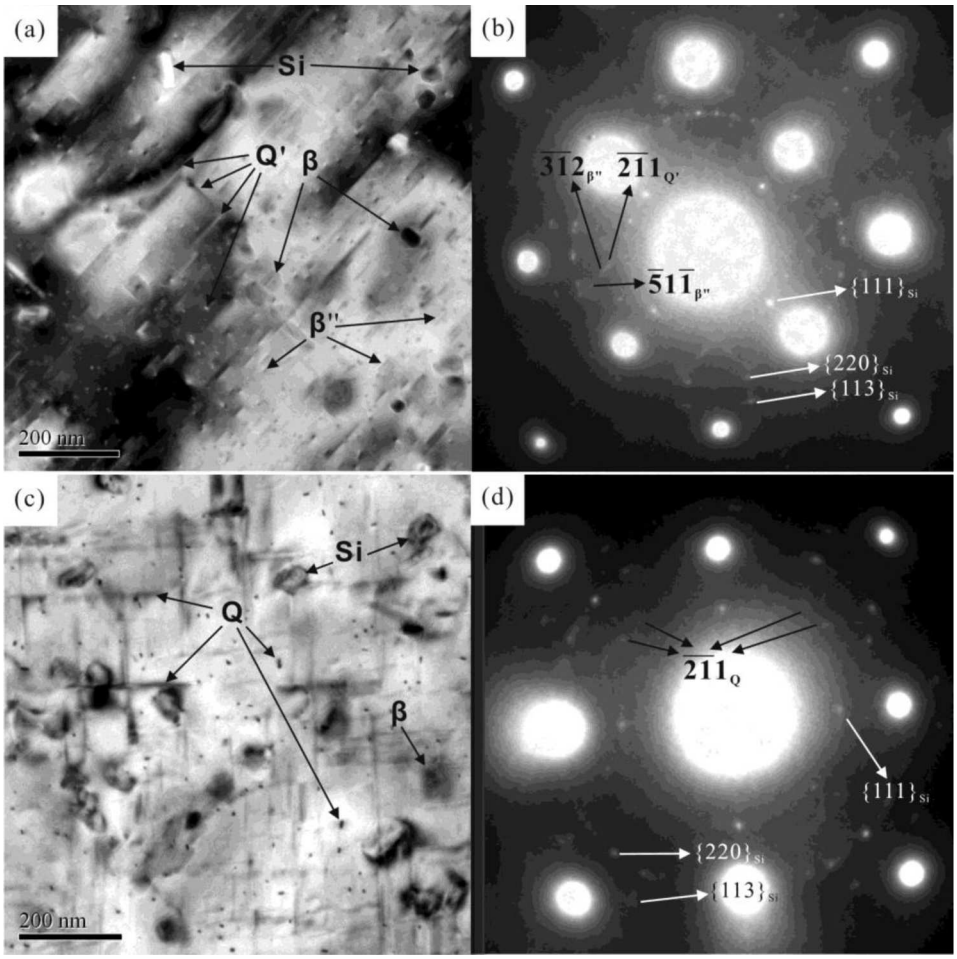

Fig. 9. TEM bright field images and SADPs of (a,b) alloy 2 aged for 120 h and (c,d) 240 h, Z = $[001]_{Al}$. Polycrystalline rings due to Si crystals are clearly observed in the SADPs

In both alloys aged for 240 h, the main precipitates are the stable phases. Only a few metastable β'' and U2 precipitates can be observed in alloy 1 aged for 240 h, as shown in Fig. 8b. The precipitates in alloy 1 aged for 208 h and 240 h (see Fig. 8) are of similar morphologies and same type, revealing the sluggish reaction rate and high thermal stability of the precipitates at this stage. Therefore the aging time of 240 h can be regarded as the final stage for both alloys.

4. Discussion

4.1. Two types of the G.P. zones: structural characteristics and their effects on aging kinetics

There are two types of the G.P. zones observed at the initial aging stage. One is the spherical G.P. zone with a diameter range of 3~4 nm, and the other is the platelet-like G.P. zone with only 1~5 layers of atoms in thickness and a diameter range of 6~12 nm. In this work, HRTEM images of both alloys aged for 5 min taken along Z = $[001]_{Al}$ (see Figs. 3c and 3d for example) reveal the diameter of spherical G.P. zones being 3~4 nm. HRTEM images of alloy 2 aged for 5 min taken along the zone axis of $[110]_{Al}$ show clearly that the platelet-like G.P. zones are parallel to $\{111\}_{Al}$ (see Fig. 5). This kind of platelet-like G.P. zone is similar in morphology to that reported by Matsuda et al. [4], but with a different habit plane of $\{111\}_{Al}$ (the habit plane is $\{001\}_{Al}$ in their work). Both the spherical and platelet-like G.P. zones observed in this work agree well with those reported in previous investigations [1-4]: only strain contrast is observed in TEM and HRTEM images (see Figs. 3 and 5), revealing that these G.P. zones are fully coherent with the Al matrix.

The β'' precipitates in alloy 2 aged for 5 h are more developed than the pre-β'' precipitates in alloy 1 aged for 10 h, as mentioned in sub-section 3.3. Thus it can be concluded that the extra trace Cu in alloy 2 has accelerated the formation of β'' precipitates. And such an acceleration effect can be attributed to the platelet-like G.P. zones which are only observed in alloy 2.

The effect of copper addition was also investigated by Murayama et al. [3] on an alloy aged at 175°C with a

composition of Al-0.55%Mg-1.26%Si-0.91%Cu (weight percent). Murayama et al. [3] found, using TEM and 3-dimensional atom probe (3DAP) that the copper element does not associate with the formation of the spherical G.P. zones but is enriched in the β'' precipitates. The spherical G.P. zones formed during pre-aging at temperatures between RT and 110°C were found to cause a retardation of the precipitation kinetics. The negative effect of this type of the spherical G.P. zone was confirmed by Serizawa et al. [31] in an Al-0.95%Mg-0.81%Si (weight percent) using methods of DSC and 3DAP. In their study, this type of spherical G.P. zone, called Cluster(1), is preferentially formed during pre-aging at around RT and hardly grows larger and would hardly dissolve at subsequent bake hardening at 170°C. Whereas in the same alloy another type of G.P. zone, called Cluster(2), with a larger size is found to have a positive effect on the dense formation of β'' precipitates. The Cluster(2) is preferentially formed by pre-aging at 100°C and remarkably grows larger with pre-aging time, and would transform into β'' precipitates, during the subsequent artificial aging treatment. This kind of positive effect was also reported by Chang et al. [32].

Based on previous studies [3, 31, 32] and the experimental results in the present work, the spherical G.P. zones observed in both alloys, i.e. Clusters(1) maintaining an diameter range of 3~4 nm, are proposed to form during the short stay at RT and would retard the precipitation kinetics, while the addition of minor Cu is proposed to cause the formation of platelet-like G.P. zones in alloy 2 at the initial stage of aging (e.g. at 5 min). These platelet-like G.P. zones, corresponding to Clusters(2), could transform to β'' precipitates and thus improve the aging kinetics. The Cu element is assumed to cooperate with Clusters(2) in some way and thus induce their formation. This is why alloy 2 acquires a microstructure of dense and fine needle-like β'' precipitates earlier than alloy 1. And such an accelerating effect on the aging kinetics becomes obvious when comparing the final states of the two alloys: the bright field image and corresponding SADP of alloy 1 aged for 240h (see Fig. 8b) reveal the existence of minor residual β'' precipitates, while in alloy 2 the β'' precipitates have almost been dissolved after aging for 240 h (see Fig. 9b).

4.2. Precipitation sequence and hardness evolution: the effect of composition

Based on the experimental results, the precipitation sequence of alloy 1 during aging treatment can be summarized as: SSSS → spherical G.P. zones → pre-β'' → β'' → U2 + Si +β_x → Si +β_x, while the precipitation sequence of alloy 2 can be expressed as: SSSS → spherical G.P. zones + platelet-like G.P. zones → pre-β'' → β'' → Q′ +β+ Si → Q +β+ Si. The minor Cu addition is found to strongly modify the precipitation sequence at the over-aged stage. Correspondingly, the hardness evolution of the alloy during aging is affected by its composition.

The hardness curves of the initial stages for both alloys show extraordinarily large fluctuations (maximum of 45.1, for alloy 1 from 30 min to 1 h) and deviations (maximum of 22.4, for alloy 1 aged for 30 min). The scatter is caused by slight heterogeneities of solute atoms and vacancy/solute complexes in the material, which result in locally varied hardness at the early stage of aging, as proposed by Chang et al. [32]. The scatter becomes smaller for the alloys aged for more than 90 h due to the homogeneous distribution of the solute atoms and precipitates after a long period of thermal diffusion and transformations. The peak aging stage occurs between 30 h to 60 h for both alloys, when the main strengthening phase is the β'' precipitates [33].

The two sharp decreases in each hardness curve reveal that there are two types of phase transformations at the over-aged stage in each alloy, from precipitates with greater hardening to precipitates with weaker hardening. According to the TEM observations and the experimental chemical compositions of the precipitates listed in Tables 1 and 2, the phase transformations in alloy 1 can be summarized as:
(1) SSSS +β'' (Mg_5Si_6) → U2 (MgAlSi) +β_x (Mg_2Si) + Si (from 60 h to 90 h);
(2) SSSS +β'' (Mg_5Si_6)+ U2 (MgAlSi) → β_x (Mg_2Si) + Si (from 120 h to 150 h).

The phase transformations in alloy 2 can be summarized as:
(1) SSSS +β'' (Mg_5Si_6) → Q′ ($Al_4CuMg_6Si_6$) + β (Mg_2Si) + Si (from 60 h to 90 h);
(2) SSSS +β'' (Mg_5Si_6)+ Q′ ($Al_4CuMg_6Si_6$) → Q ($Al_4Cu_2Mg_8Si_7$)+ β (Mg_2Si) + Si (from 120 h to 150 h).

The occurrence of Q′/Q precipitates in alloy 2 containing 0.1 wt.% Cu is consistent with the investigation of Chakrabarti et al. [34]. It is found that the hardness values of alloy 2 are higher than those of alloy 1 by 4.25 on average after aging time of 90 h, in agreement with the hardness measurements of Miao and Laughlin [23] for two 6022 alloys containing 0.07% Cu and 0.91% Cu (weight percent). In their work, the alloy with higher Cu content presented higher strengthening response. This phenomenon is caused by the greater strengthening effect of the lath-like Q′ and Q precipitates, and the reduction in the amount of less strengthening Mg_2Si and Si platelet-like precipitates due to the Si atoms entering into the Q′/Q precipitates.

5. Conclusions

The precipitation sequences of two as-cast Al-Mg-Si 6005 alloys (containing no Cu or 0.10 wt.% Cu) during aging treatment at 150°C were investigated. It has been shown that the precipitation sequence of the Cu-free Al-Mg-Si alloy during aging treatment can be summarized as: SSSS → spherical G.P. zones → pre-β'' → β'' → U2 + Si +β_x → Si +β_x, while the precipitation sequence of the other alloy is greatly modified by the minor Cu addition as: SSSS → spherical G.P. zones + platelet-like G.P. zones → pre-β'' → β'' → Q′ + β + Si → Q +β+ Si. A new type of β precipitate with a special orientation in the Al matrix, named as β_x in this work, is found in the Cu-free alloy. The addition of minor Cu causes the formation of platelet-like G.P. zones along $\{111\}_{Al}$ planes in the alloy, which have a positive effect on the precipitation kinetics. Moreover, the extra Cu content increases the hardening effect at the over-aged stage due to the formation of Q′ and Q precipitates, and the reduction in the amount of β and Si precipitates.

Acknowledgements

This work is financially supported by Natural Science Foundation of China (No. 50831007), Creative Research Group of National Natural Science Foundation of China (No. 51021063) and Fundamental Research Funds for the Central Universities (2011JQ021).

REFERENCES

[1] M. Murayama, K. Hono, M. Saga, M. Kikuchi, Atom probe studies on the early stages of precipitation in Al-Mg-Si alloys, Mater. Sci. Eng. **A 250**, 127-132 (1998).

[2] M. Murayama, K. Hono, Pre-precipitate clusters and precipitation processes in Al-Mg-Si alloys, Acta Mater. **47**, 1537-1548 (1999).

[3] M. Murayama, K. Hono, W.F. Miao, D.E. Laughlin, The effect of Cu additions on the precipitation kinetics in Al-Mg-Si alloy with excess Si, Metall. Mater. Trans. **A 32A**, 239-246 (2001).

[4] K. Matsuda, H. Gamada, K. Fujii, Y. Uetani, T. Sato, A. Kamio, S. Ikeno, High-resolution electron microscopy on the structure of Guinier-Preston zones in an Al-1.6 mass pct Mg_2Si alloy, Metall. Mater. Trans. **A 29A**, 1161-1167 (1998).

[5] C.D. Marioara, S.J. Andersen, J. Jansen, H.W. Zandbergen, Atomic model for GP zones in a 6082 Al-Mg-Si system, Acta Mater. **49**, 321-328 (2001).

[6] S.J. Andersen, H.W. Zandbergen, J. Jansen, C. Træholt, U. Tundal, O. Reiso, The crystal structure of the β'' phase in Al-Mg-Si alloys, Acta Mater. **46**, 3283-3298 (1998).

[7] H.S. Hasting, A.G. Frøseth, S.J. Andersen, R. Vissers, J.C. Walmsley, C.D. Marioara, F. Danoix, W. Lefebvre, R. Holmestad, Composition of β'' precipitates in Al-Mg-Si alloys by atom probe tomography and first principles calculations, J. Appl. Phys. **106**, 123527-123536 (2009).

[8] K. Matsuda, T. Naoi, K. Fujii, Y. Uetani, T. Sato, A. Kamio, S. Ikeno, Crystal structure of the β'' phase in an Al-l.0mass%Mg2Si-0.4mass%Si alloy, Mater. Sci. Eng. **A 262**, 232-237 (1999).

[9] R. Vissers, M.A. van Huis, J. Jansen, H.W. Zandbergen, C.D. Marioara, S.J. Andersen, The crystal structure of the β' phase in Al-Mg-Si alloys, Acta Mater. **55**, 3815-3823 (2007).

[10] K. Matsuda, Y. Sakaguchi, Y. Miyata, Y. Uetani, T. Sato, A. Kamio, S. Ikeno, Precipitation sequence of various kinds of metastable phases in Al-1.0mass% Mg2Si-0.4mass% Si alloy, J. Mater. Sci. **35**, 179-189 (2000).

[11] S.J. Andersen, C.D. Marioara, R. Vissers, A. Frøseth, H.W. Zandbergen, The structural relation between precipitates in Al-Mg-Si alloys, the Al-matrix and diamond silicon, with emphasis on the trigonal phase U1-MgAl2Si2, Mater. Sci. Eng. **A 444**, 157-169 (2007).

[12] S.J. Andersen, C.D. Marioara, A. Frøseth, R. Vissers, H.W. Zandbergen, Crystal structure of the orthorhombic U2-$Al_4Mg_4Si_4$ precipitate in the Al-Mg-Si alloy system and its relation to the β' and β'' phases, Mater. Sci. Eng. **A 390**, 127-138 (2005).

[13] K. Matsuda, S. Ikeno, T. Sato, A. Kamio, Classification of metastable phases in Al-Mg_2Si alloys by HRTEM, Mater. Sci. Forum **217-222**, 707-712 (1996).

[14] K. Matsuda, Y. Uetani, T. Sato, S. Ikeno, Metastable phases in an Al-Mg-Si alloy containing copper, Metall. Mater. Trans. **A 32A**, 1293-1299 (2001).

[15] L. Arnberg, B. Aurivillius, The crystal structure of $Al_xCu_2Mg_{12-x}Cu_7$, (h-AlCuMGSi), Acta. Chem. Scand. **A 34**, 1-5 (1980).

[16] L. Sagalowicz, G. Lapasset, G. Hug, Transmission electron microscopy study of a precipitate which forms in the Al-Mg-Si system, Phil. Mag. Lett. **74**, 57-66 (1996).

[17] E.N. Nikitin, E.N. Tkalenko, V.K. Zaitsev, A.I. Zaslavskii, A.K. Kuznetsov, Phase diagram and some properties of solid solutions in a Mg2Si-Mg2Sn system, Izv. Akad. Nauk SSSR Neorg. Mater. **4**, 1902-1906 (1968).

[18] K. Matsuda, Y. Ishida, I. Müllerová, L. Frank, S. Ikeno, Cube-phase in excess Mg-type Al-Mg-Si alloy studied by EFTEM, J. Mater. Sci. **41**, 2605-2610 (2006).

[19] K. Matsuda, T. Kawabata, Y. Uetani, T. Sato, S. Ikeno, Hexagonal tabular β-phase in Al-Mg-Si-Cu alloy, Scripta Mater. **47**, 467-471 (2002).

[20] Silicon, PDF 00-27-1402, Monograph 25, National Bureau of Standards (US) **13**, 35 (1976).

[21] C.D. Marioara, S.J. Andersen, A. Birkeland, R. Holmestad, Orientation of silicon particles in a binary Al-Si alloy, J. Mater. Sci. **43**, 4962-4971 (2008).

[22] C.D. Marioara, H. Nordmark, S.J. Andersen, R. Holmestad, Post-β'' phases and their in?uence on microstructure and hardness in 6xxx Al-Mg-Si alloys, J. Mater. Sci. **41**, 471-478 (2006).

[23] W.F. Miao, D.E. Laughlin, Effects of Cu content and preaging on precipitation characteristics in Aluminum alloy 6022, Metall. Mater. Trans. **A 31A**, 361-371 (2000).

[24] K. Matsuda, D. Teguri, Y. Uetani, Y. Sato, S. Ikeno, Cu-segregation at the Q′/α-Al interface in Al-Mg-Si-Cu alloy, Scripta Mater. **47**, 833-837 (2002).

[25] M. Jin, J. Li, G. Shao, Study of Cu addition on precipitation behaviors and mechanical properties in AA6082 Al-Mg-Si alloy, Mater. Sci. Forum **546-549**, 825-828 (2007).

[26] J. Man, L. Jing, S.G. Jie, The effects of Cu addition on the microstructure and thermal stability of an Al-Mg-Si alloy, J. Alloys Compd. **437**, 146-150 (2007).

[27] G.C. Weatherly, A. Perovic, N.K. Mukhopadhyay, D.J. Lloyd, D.D. Perovic, The precipitation of the Q phase in an AA6111 alloy, Metall. Mater. Trans. **A 32A**, 213-218 (2001).

[28] K. Li, M. Song, Y. Du, H. Zhang, Simulation of the electron diffraction patterns from needle/rod-like precipitates in Al-Mg-Si alloys, Mater. Charact., accepted (2011).

[29] J.H. Chen, E. Costan, M.A. van Huis, Q. Xu, H.W. Zandbergen, Atomic pillar-based nanoprecipitates strengthen AlMgSi alloys, Science **312**, 416-419 (2006).

[30] R.S. Yassar, D.P. Field, H. Weiland, The effect of predeformation on the β'' and β' precipitates and the role of Q′ phase in an Al-Mg-Si alloy; AA6022, Scripta Mater. **53**, 299-303 (2005).

[31] A. Serizawa, S. Hirosawa, T. Sato, Three-dimensional atom probe characterization of nanoclusters responsible for multistep aging behavior of an Al-Mg-Si alloy, Metall. Mater. Trans. **A 39A**, 243-251 (2008).

[32] C.S.T. Chang, I. Wieler, N. Wanderka, J. Banhart, Positive effect of natural pre-ageing on precipitation hardening in Al-0.44 at% Mg-0.38 at% Si alloy, Ultramicroscopy **109**, 585-592 (2009).

[33] S.K. Son, S. Matsumura, K. Fukui, M. Takeda, The compositions of metastable phase precipitates observed at peak hardness condition in an Al-Mg-Si alloy, J. Alloys Compd. **509**, 241-245 (2011).

[34] D.J. Chakrabarti, D.E. Laughlin, Phase relations and precipitation in Al-Mg-Si alloys with Cu additions, Prog. Mater. Sci. **49**, 389-410 (2004).

Received: 20 November 2011.